Dyes and Pigments 93 (2012) 1488–1497

Contents lists available at SciVerse ScienceDirect

Dyes and Pigments

journal homepage: www.elsevier.com/locate/dyepig

Structural planarity and conjugation effects of novel symmetrical acceptor–donor–acceptor organic sensitizers on dye-sensitized solar cells

Hsuan-Chih Chu [a], Duryodhan Sahu [a], Ying-Chan Hsu [b], Harihara Padhy [a], Dhananjaya Patra [a], Jiann-T'Suen Lin [b], Dibyendu Bhattacharya [b], Kuang-Lieh Lu [b], Kung-Hwa Wei [a], Hong-Cheu Lin [a,*]

[a] Department of Materials Science and Engineering, National Chiao Tung University, Hsinchu 30049, Taiwan, ROC
[b] Institute of Chemistry, Academia Sinica, Taipei 115, Taiwan, ROC

ARTICLE INFO

Article history:
Received 20 May 2011
Received in revised form
14 September 2011
Accepted 20 September 2011
Available online 4 November 2011

Keywords:
Carbazole
Solar cell
Sensitizer
Donor–acceptor
Density functional theory
Charge transfer

ABSTRACT

In this study two series of novel symmetrical acceptor–donor–acceptor organic sensitizers containing 3,6- and 2,7-functionalized carbazole cores, respectively, connected to two anchoring cyanoacrylic acid termini via thienyl linkers were synthesized. The effect of the molecular planarity originating from the 3,6- and 2,7-functionalized carbazole cores on the performance of corresponding solar cells were investigated. Molecular orbital analyses revealed the characteristics of the carbazole-based highest occupied molecular orbitals and acid-based lowest unoccupied molecular orbitals. Time-dependent density functional theory calculations allowed us to assign the electronic transitions (>90%) of the low energy bands. Among these new dyes, the highest power conversion efficiency of 4.82% was obtained in a dye-sensitized solar cell device under standard AM 1.5 sunlight with an open-circuit voltage of 0.61 V, a short-circuit photocurrent density of 12.66 mA cm^{-2} and a fill factor of 0.62.

1. Introduction

Solar energy has proven capacity to match the world's increasing energy needs [1,2]. Although several types of inorganic and organic materials, including semiconductors [3–6] and conducting polymers [7–13], have been applied in solar cell applications, dye-sensitized solar cells (DSSCs) developed initially by O'Regan and Grätzel in 1991 [14], are among the cheapest alternatives to established solar cells. In DSSCs, the combination of nanocrystalline TiO_2 with charge-transfer sensitizers provides a sufficient surface area for efficient light harvesting. Devices incorporating classic ruthenium complexes have already reached solar-to-electrical energy conversion efficiencies up to 11% under AM 1.5 irradiation conditions, with impressive long term stability [15–19]. Nevertheless, the use of ruthenium dyes, which have with relatively low molar extinction coefficients, and the need for rare and expensive metals with tedious purification processes are major problems in terms of cost and environmental issues, hampering the large-scale applications of such solar cells. Fully organic dyes can exhibit superior π–π^* charge transfer (CT) and intramolecular charge transfer (ICT) transitions relative to those of their ruthenium-based metal–ligand counterparts, in their absorption spectra, with high molar extinction coefficients [20]. Therefore, organic dyes are receiving increasing attention as alternatives to ruthenium-based dyes for DSSC applications.

The wide interest in the application of organic dyes in DSSCs is due primarily to their structural flexibility at the molecular level [21], their tunable optical properties [22], their lower degrees of aggregation, and their potentially high dye loadings [23]. Several groups have developed metal-free organic sensitizers containing two anchoring groups at their two termini, such that they adsorb flat onto TiO_2 surfaces [24]. To double the light absorption efficiency and minimize dye aggregation, Wong and co-workers recently introduced two electron donor–acceptor branches into the rigid cross-shaped molecular structure, with two anchoring carboxylate acceptors (to improve dye adsorption and to direct photoinduced electron injection) and two diphenylamine donors, of a spirobifluorene-based DSSC dye to achieve an overall power conversion efficiency (PCE) of 3.75% [25]. Although 3,6-carbazole moieties have become promising units for organic dyes in practical DSSC applications in recent years [26,27], 2,7-functionalized carbazole units—widely used planar conjugated segments [13]—have been neglected for use in DSSC dyes. Therefore, in this study we sought to integrate various central carbazole donors with two terminal

* Corresponding author. Tel.: +8863 5712121x55305; fax: +8863 5724727.
E-mail address: linhc@cc.nctu.edu.tw (H.-C. Lin).

0143-7208/$ – see front matter © 2011 Elsevier Ltd. All rights reserved.
doi:10.1016/j.dyepig.2011.09.012

acid acceptors for the design of organic DSSC dyes. To the best of our knowledge, no previous reports have described organic DSSC dyes containing functionalized carbazole donor units with two terminal cyanoacrylic acids.

In this paper, we report two sets of novel symmetrical acceptor–donor–acceptor organic sensitizers (Fig. 1) featuring electron-donating carbazole cores functionalized at two different positions (i.e., 3,6- and 2,7-substituted) and linked through π-conjugated thiophene bridges (to broaden the absorption range of the dyes) to two electron-accepting cyanoacrylic acid units acting as terminal anchoring groups. Furthermore, we introduced hexyl and branched-octyl groups into the central 3,6- and 2,7-carbazole moieties, respectively, to generate sterically hindered cores and, thereby, minimize dye aggregation and maximize adsorption onto TiO_2 surfaces [28]. The linking of such electron donor and acceptor groups via conducting thiophene units in organic DSSC dyes allowed us to examine the effects of (i) the planarity of the central electron-donating carbazole moieties with 3,6- and 2,7-substitution patterns and (ii) the number (two or three) of conjugated thienyl groups (with or without hexyl side chains) on the photovoltaic performance of the organic DSSC dyes. Structure-based density functional theory (DFT) calculations confirmed that the efficiencies of these dyes depended on the coplanarity of the carbazole donor groups with respect to the thiophene units. Molecular orbital analyses revealed an ideal distribution of electrons, with the highest occupied molecular orbital (HOMO) and lowest unoccupied molecular orbital (LUMO) associated with the carbazole- and acid-based characteristics, respectively. In addition, the conducting thiophene linkers were essential for strong conjugation across the electron donor–acceptor systems. Thus, we confirmed that both the sites of functionalization of the central carbazole units and the number of bridging thiophene units (with or without lateral alkyl chains) play key roles affecting the spectral responses and dye adsorption densities on TiO_2 surfaces [26,28], making them critical factors influencing the efficiencies of DSSC dyes.

2. Experimental

2.1. Materials

Chemicals and solvents were purchased in reagent grades from Aldrich, ACROS, TCI, Strem, Fluka, and Lancaster Chemical. Prior to use, THF and CH_2Cl_2 were freshly distilled over Na/benzophenone and CaH_2, respectively. Tetra-*n*-butylammonium hexafluorophosphate ($TBAPF_6$) was recrystallized twice from absolute EtOH and further dried for two days under vacuum. *N*-Bromosuccinimide was recrystallized from distilled water and dried under vacuum. All other chemicals were used without further purification. The synthetic routes and detailed procedure for the preparation of dyes **M1**–**M6** are presented in Schemes S1 and S2 and are described in the Supporting information. The chemical structures of all products were confirmed using ^1H NMR spectroscopy and mass spectrometry (FAB) and through elemental analyses.

2.2. Characterization

^1H NMR spectra were recorded on a Varian unity 300 MHz spectrometer with d_6-DMSO and $CDCl_3$ as solvents. Elemental analyses were performed on a HERAEUS CHN-OS RAPID elemental analyzer. UV–Visible absorption spectra were recorded in dilute THF solutions (10^{-5} M) on a HP G1103A spectrophotometer, and photoluminescence (PL) spectra were obtained on a Hitachi F-4500 spectrophotometer. Cyclic voltammetry (CV) measurements were performed using a BAS 100 electrochemical analyzer with a standard three-electrode electrochemical cell in a 0.1 M tetrabutylammonium hexafluorophosphate ($TBAPF_6$) solution (in THF) at room temperature with a scanning rate of 100 mV/s. During CV measurements, the solutions were purged with nitrogen for 30 s. In each case, a carbon as working electrode, a platinum wire as the counter electrode, and a silver wire as the quasi-reference electrode were used, and Ag/AgCl (3 M KCl) electrode was served as a reference electrode for all potentials quoted herein. The redox couple of the ferrocene/ferrocenium (Fc/Fc^+) ion was used as an external standard. The corresponding HOMO and LUMO levels were calculated from the value of $E_{ox/onset}$ (onset oxidation potential) and from the UV–Vis absorption, respectively.

2.3. Device fabrication

2.3.1. TiO_2 paste preparation

The preparation of TiO_2 precursor and the electrode fabrication were performed based on a previous report [29] at an autoclaved temperature of 240 °C. The precursor solution was prepared as follows: The precursor solution was prepared as follows: 0.1 M HNO_3 (430 mL) was slowly mixed with $Ti(C_3H_7O)_4$

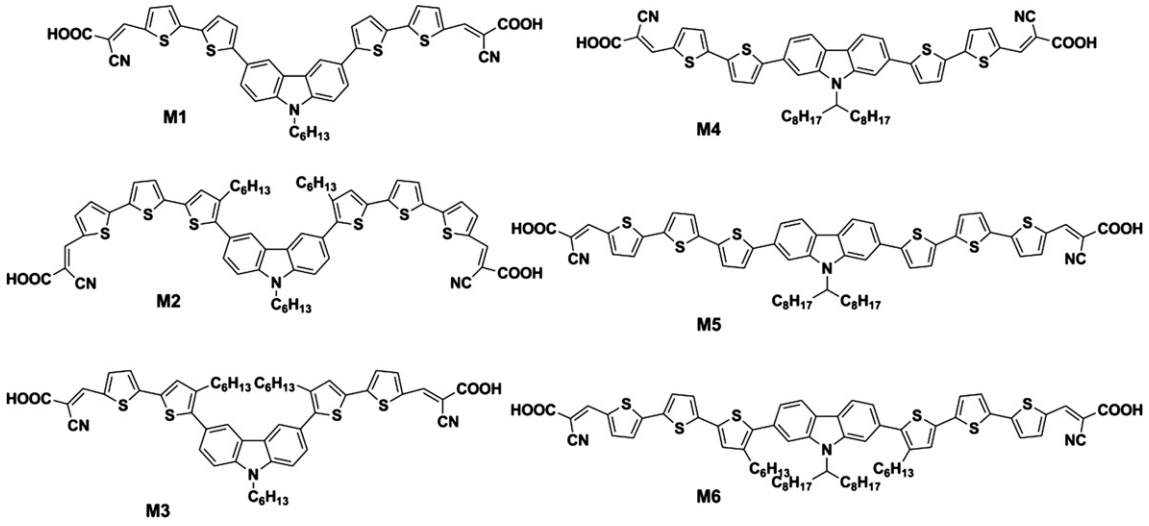

Fig. 1. Structures of organic dyes (**M1**–**M6**).

(72 mL) under vigorous stirring to form a mixture. After hydrolysis, the mixture was stirred vigorously while heating at 85 °C in a water bath for 8 h to achieve peptization. When the mixture was cooled to room temperature, the resultant colloid was filtered and the filtrate then heated in an autoclave at 240 °C for 12 h to grow the TiO_2 particles. When the colloid was cooled to room temperature, it was vibrated ultrasonically for 10 min. The TiO_2 colloid was concentrated to 13 wt%, followed by the addition of 30 wt% (with respect to TiO_2 weight) of poly(ethylene glycol) (PEG; MW = 20,000 g mol^{-1}) to prevent the film from cracking while drying.

2.3.2. Fabrication of DSSC devices

The TiO_2 paste was deposited onto a FTO glass substrate with a dimension of 0.5 × 0.5 cm^2 using the glass rod method. Polyester tape (3 M) was used as an adhesive on two edges of the FTO glass. The tape was removed after the TiO_2 paste had been spread onto the FTO using a glass rod, and the TiO_2 paste was then air dried at room temperature for 1 h. The TiO_2-coated FTO was heated to 500 °C at a heating rate of 10 °C/min and maintained for 30 min before cooling to room temperature. After repeating the procedure to control the thickness of TiO_2 film, the final coating was applied using a TiO_2 paste containing 300- and 20-nm-diameter light scattering TiO_2 particles (30 and 70 wt%, respectively) and then the sample was heated at 500 °C. The thicknesses of the TiO_2 films were measured using a Dektak3 profilometer (Veeco/Sloan Instruments). The density of each adsorbed dye was calculated from the concentration difference of each solution before and after immersion of the TiO_2 film. The TiO_2 electrode having an area of 0.25 cm^2 was immersed overnight in a MeCN/*tert*-butanol mixture (1:1, v/v) containing 3×10^{-4} M *cis*-di(thiocyanato)bis(2,2′-bipyridyl-4,4′-dicarboxylato) ruthenium(II) bis(tetrabutylammonium) (N719, Solaronix SA) or in a THF solution containing 3×10^{-4} M of the organic sensitizer. Thermally platinized FTO was used as a counter electrode; it had an active area of 0.36 cm^2 and was adhered using 60-μm-thick polyester tape. After rinsing with MeCN or THF, the photoanode was placed on top of the counter electrode and tightly clipped together to form a cell. Finally, the electrolyte was then injected into the space and then the cell was sealed with Torr Seal cement (Varian). The electrolyte comprised 0.5 M LiI, 0.05 M I_2, and 0.5 M 4-*tert*-butylpyridine (TBP) dissolved in MeCN.

2.4. Measurements

A 0.6 × 0.6 cm cardboard mask was clipped onto the device to constrain the illumination area. Photoelectrochemical characterization on the solar cells was performed using an Oriel Class A solar simulator (Oriel 91195A, Newport). The photocurrent–voltage characteristics of the DSSCs were measured using a potentiostat/galvanostat (CHI650B, CH Instruments) at a light intensity of 1.0 sun, calibrated using an Oriel reference solar cell (Oriel 91150, Newport). The monochromatic quantum efficiencies were recorded through a monochromator (Oriel 74100, Newport) under short-circuit conditions. The intensity at each wavelength was in the range from 1 to 3 mW cm^{-2}. The photovoltage transients of assembled devices were recorded using a digital oscilloscope (LeCroy, WaveSurfer 24Xs). Pulsed laser excitation was applied by a Q-switched Nd:YAG laser (Continuum, model Minilite II) with a 1 Hz repetition rate at 532 nm and a 5-ns pulse width at half-height. The beam size was slightly larger than 0.5 × 0.5 cm^2 to cover the area of the device. The photovoltage of each device was adjusted to 50 mV by varying the incident pulse energy. The average electron lifetime was estimated by fitting the decay of the open-circuit voltage transient with $\exp(-t/\tau_R)$, where t is time and τ_R is recombination lifetime.

2.5. Quantum chemistry computation

The predicted structures of the molecules were optimized using B3LYP hybrid functional [30] and 6-31G* basis sets [31]. For each of the molecules, a number of conformational isomers were examined, and the one with the lowest energy was used. To determine the excited states, time-dependent density functional theory (TD-DFT) was employed with the B3LYP functional. The lowest 33 singlet–singlet excited states were calculated using TD-DFT (up to an energy of that with ca. 250 nm). Solvation effect was investigated performing TD-DFT calculations in THF solvent with the nonequilibrium version of the conductor-like polarizable continuum model (C-PCM) method with dielectric constant of 7.58 using same basis set and functional, and the detailed result is illustrated in Fig. S4 of the Supporting information. All of the analyses were performed using the Gaussian 03 (G03) (revision E.01) program package [32] and DFT. Finally, based on the compound results, the stereo-contour graphs of some related frontier molecular orbitals of the complexes for the ground states were drawn using the GView 3.09 program. Simulated spectra with the oscillator strength (f) values were obtained with the program GaussSum 2.1.2 [33].

3. Results and discussion

3.1. Optical properties

Fig. 2a and b display the UV–Vis absorption and normalized PL spectra, respectively, of the dyes **M1**–**M6** (10^{-5} M in THF); Table 1 summarizes the data. In general, all dyes showed two prominent absorption bands: (a) a small absorption band at λ_{max} of 312–387 nm, which attributed to the localized π–π^* transition, and (b) a large absorption band in the visible region, corresponding to an ICT transition from the central electron-donating carbazole unit to both electron-accepting cyanoacrylic acid termini, consistent with the theoretical data (Fig. 2c). Because of their structural similarities, **M1**–**M6** exhibited similar ICT transition peaks located in the range (λ_{max}) from 455 to 484 nm, with molar extinction coefficients (ε, at the maximum absorption wavelength λ_{max}) in the range from 5.85×10^4 to 10.24×10^4 M^{-1} cm^{-1}.

The wide absorption ranges of **M1**–**M6** and their high molar extinction coefficients, relative to that of N719 dye (ε = ca. 14,000 M^{-1} cm^{-1}) [15b] suggested that these dyes had potential for use as efficient materials in DSSC applications. All of these dyes exhibited weak emissions with a Stokes shift of ca. 120 nm in THF solutions; they also displayed consistent red-shifted absorptions and emissions upon increasing the number of thiophene units. For instance, red shifts occurred upon increasing the number of conjugated thiophene units from **M3** to **M2** and from **M4** to **M5** (in the 3,6- and 2,7-functionalized carbazole-based systems), respectively. As expected, elongation of the π-conjugation length decreased the π–π^* band gap energy and led to spectral red shifts of the π–π^* transitions. Furthermore, substitution of the alkyl side chains in the thiophene moieties, from **M1** to **M3** and from **M5** to **M6**, led to intramolecular ring twisting, thereby inducing larger band gap energies and associated blue shifts of 14–15 nm in the UV–Vis spectra. Therefore, at a set number of thiophene units and with a fixed structure for the carbazole donor moiety, the number of alkyl side chains of the dyes could effectively influence the features in the absorption spectra [34].

In contrast to the coplanar structures of the 2,7-functionalized carbazole donor centers in **M4** and **M6**, the nonplanar structure of the 3,6-functionalized carbazole donor centers in **M1** and **M2** induced blue shifts in both the (a) and (b) bands in the UV–Vis spectra. As indicated in Fig. 2a, the dyes **M3** and **M5** had the shortest and longest absorption wavelengths, respectively, due to

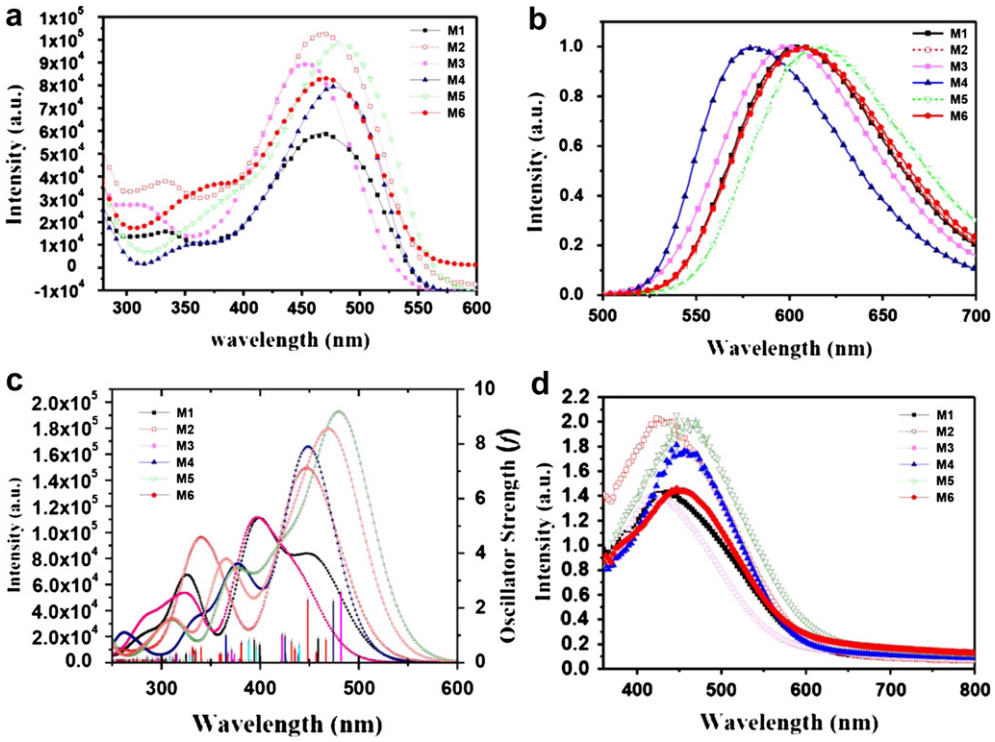

Fig. 2. (a) UV–Vis absorption and (b) normalized emission spectra of dyes recorded in THF solutions (concentration: 1.0×10^{-5} M). (c) Calculated (B3LYP/6-31G*) absorption spectra and oscillation strengths and (d) absorption spectra of the dyes on 1.5-μm-thick TiO_2 surfaces.

(i) the planarity of the central (3,6- and 2,7-functionalized) carbazole unit, (ii) the number (two and three) of bridging thiophene units, and (iii) the degree of twisting induced by the lateral alkyl chains. In general, the characteristics of ICT bands depend on the nature of the electron donors and acceptors as well as the spacers between the donors and acceptors. **M2** and **M5** had higher extinction coefficients (ε), consistent with the literature report suggesting that the ICT transitions of conjugated molecules will provide higher extinction coefficients upon increasing the conjugation length [35], resulting in greater degrees of light harvesting and increased photocurrent response [36]. Fig. 2d presents the absorption spectra of the dyes adsorbed onto a TiO_2 surface at a thickness of 1.5 μm. The signals in the absorption spectra of the dyes on the TiO_2 films were distinctly broadened (extended to longer wavelength) relative to those in the absorption spectra of their THF solutions (Fig. 2a). Although the broader absorptions of the dyes on the TiO_2 films are favorable for light harvesting, their absorption maxima were shifted to shorter wavelengths; we attribute these blue shifts to the formation of H-type aggregates or deprotonation of the carboxylic acid units, indicating that the carboxylic acid moieties are stronger electron acceptors compared with the carboxylate-titanium units. Similar phenomena have been observed for several other organic dyes [37]. We estimated the amounts of dye adsorbed on the TiO_2 surface (Table 1) from the difference in the concentrations of each solution before and after immersion of the TiO_2 sample, followed by rinsing with THF to avoid miscounting the dye molecules physically adsorbed onto the film. The nonplanar structures of the dyes featuring central carbazole units suppressed their aggregation after anchoring to the TiO_2 surfaces, meaning that the dye molecules were adsorbed strongly to the TiO_2 surfaces [38,39]; as a result, we obtained high dye densities for **M1** and **M3** (Table 1). In contrast, because of its larger number of conjugated thiophene groups, **M2** underwent aggregation to a greater degree, decreasing the amount of dye adsorbed

Table 1
Optical and electrochemical properties of the dyes.

Dye	λ_{max}^{Abs} (nm)[a] ($\varepsilon \times 10^4$, M^{-1} cm^{-1})	λ_{max}^{Abs} (nm)[b] (on TiO_2)	λ_{max}^{Em} (nm)[a]	E_g^{opt} (eV)[c]	E_{HOMO} (eV)[d]	E_{LUMO} (eV)[d]	Calculated band gap (eV)	Dye adsorption (mol/cm^2)[e]
M1	331 (1.58), 470 (5.85)	434	606	2.15	−5.40	−3.25	2.19	2.4×10^{-7}
M2	331 (3.78), 468 (10.24)	427	606	2.19	−5.38	−3.19	2.23	1.6×10^{-7}
M3	312 (2.83), 455 (8.92)	421	600	2.27	−5.37	−3.10	2.32	3.0×10^{-7}
M4	353 (1.00), 480 (7.96)	457	582	2.18	−5.52	−3.34	2.18	2.2×10^{-7}
M5	387 (3.14), 484 (9.79)	458	617	2.11	−5.37	−3.26	2.13	1.5×10^{-7}
M6	374 (3.61), 470 (8.25)	449	610	2.17	−5.49	−3.32	2.20	2.1×10^{-7}

[a] Absorption and emission wavelengths measured in THF solutions (10^{-5} M).
[b] Absorption spectra of the dyes on 1.5 μm TiO_2 films.
[c] Optical band gaps calculated from absorption onsets ($E_g^{opt} = 1240/\lambda$ edge).
[d] HOMO = [−(E_{onset} − 0.45) − 4.8] eV where 0.45 V is the value for ferrocene vs. Ag/Ag^+ and 4.8 eV is the energy level of ferrocene below the vacuum and LUMO levels of the dyes calculated by subtraction of the optical banpgaps from the E_{HOMO} values.
[e] Dyes adsorbed on TiO_2 surfaces with a thickness of 15 μm (the same film made for the device fabrication).

and, therefore, resulting to the lowest degree of dye adsorption among **M1**–**M3** (with the same nonplanar 3,6-carbazole moiety).

On the other hand, among **M4**–**M6** (with the same coplanar 2,7-carbazole moiety), **M4** had the lowest degree of aggregation, thereby leading to the highest amount of dye adsorption. Because extended conjugation led to greater degrees of aggregation, the presence of more thiophene units in **M2** than in **M3** (in the 3,6-carbazole system) and in **M5** than in **M4** (in the 2,7-carbazole system) resulted in lower amounts of dye adsorbing on the TiO_2 surfaces. Moreover, substituting alkyl side chains onto the thiophene units of **M1** and **M5** to form **M3** and **M6**, respectively, induced lower degrees of aggregation (as a result of lateral alkyl chain twisting) and, thereby, greater dye adsorption on the TiO_2 surfaces. Therefore, in contrast to the nonplanar structures of **M1** and **M2** (bearing 3,6-carbazole cores), the coplanar structures of **M4** and **M6** (containing 2,7-carbazole cores) resulted in higher dye adsorption. Overall, we observed similar structural influences on the absorption wavelengths and intensities for all of these organic dyes. Accordingly, changes in the number (two or three) of thiophene units, the presence or absence of alkyl side chains, and the substitution pattern (2,7 or 3,6) of the carbazole core all influenced the net light harvesting ability and the spectral responses—suggesting that they would also ultimately affect the photovoltaic properties.

3.2. Quantum-chemical calculations

To gain insight into the geometrical electronic structures of the dyes, we performed DFT calculations using the Gaussian 03 program package. As representative examples, Fig. 3 presents the optimized geometries of the ground states and electronic distributions of the HOMOs and LUMOs of **M1** and **M2** [see Fig. S2 (Supporting information) for those of the other dyes]. We obtained computed values for the angles formed between the carbazole and thiophene planes in **M2** and **M6** of 38.3 and 37.2°, respectively; the other congeners, however, displayed good conjugation between their donor and conductor units [see Table 2 and Fig. S1 (Supporting information)]. Furthermore, in their transoid arrangements, the conducting thiophene units were also coplanar, with extensive π delocalization. These were lower in energy than their cisoid counterparts, except for **M2**, where they were in different planes. We also noticed that the terminal 2-cyanoacrylic acid groups were found to be coplanar with their adjacent thiophene units—except in **M2** and **M6**, where the angles between the planes were greater than 14° [40]. We also analyzed

Table 2
Dihedral angles (°) of **M1**–**M6** dyes between the carbazole and thiophene moieties, between two neighboring aromatic rings, and between the aromatic ring and 2-cyanoacrylic acid moiety.[a]

Dihedral angle	M1	M2	M3	M4	M5	M6
σdonor–σconductor[b]	0.59	38.4	1.33	0.78	0.40	37.2
Σconductor–σconductor[b]	0.22	14.7	0.79	0.20	0.07	0.24
Σconductor–σacceptor[b]	0.21	14.4	0.23	0.06	0.44	14.6

[a] Modeled-structures were obtained from DFT calculations.
[b] Donor = carbazole unit, conductor = thiophene unit, acceptor = cyanoacrylate unit.

the electronic structures of the dyes in vacuum. Fig. S2 (Supporting information) provides a schematic representation of the energy levels of the frontier molecular orbitals of **M1**–**M6**. The HOMOs of all sensitizers were delocalized over the carbazole moieties, with major components arising from the nitrogen atoms, with sizable contributions from the π frameworks of the surrounding ligands. All of the HOMO-1 electron densities were spread over the thiophene and 2-cyanoacrylic acid moieties. The LUMOs were defined by the π^* orbitals, delocalized over the thiophene moieties and cyanoacrylic acid units. In DSSCs, such ideal delocalization should facilitate injection of electrons from the excited dyes to the conduction bands and also minimize the recombination of injected electrons in the conduction bands with the oxidized dyes [41]. Moreover, the overlapping of both the HOMO and LUMO energy levels in the π-bridged thiophene affords strong oscillation strength (Fig. 2c), enhancing the electronic transition dipole moments between the vibrational energy levels. This situation is in accordance with the Franck–Condon principle; the bridging thiophene unit is the key element for high molar extinction coefficients [42]. In the **M2** sensitizer, however, the HOMO and LUMO densities were both localized on the π-bridge and the acceptor. Thus, we suspected that poor charge generation would hinder the overall efficiency of its DSSCs [43]. The introduction of additional thiophene units stabilized the LUMO energy levels through increased conjugation. Alkyl substitution, however, destabilized the LUMOs of **M2** and **M6**. The calculated relative energies (Fig. 4) were consistent with the experimental values calculated from the electrochemical and spectroscopic data (*vide infra*). Fig. 2c displays the computed ground state vertical excitation energies with oscillator strengths greater than 0.1; the TD-DFT data were consistent with the experimental electronic spectra. The two electronic transitions with lowest energy levels (HOMO→LUMO and HOMO-1→LUMO) had the highest oscillator strengths (*f*), with significant degrees of

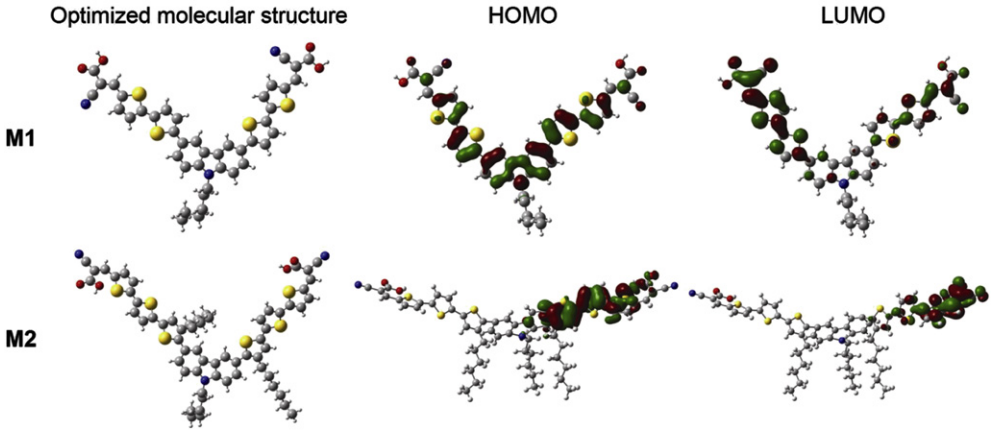

Fig. 3. Graphical representations of the frontier orbitals of the dyes **M1** and **M2** computed at the DFT/B3LYP/6-31G* level of theory. Atom coloring: yellow, sulfur; gray, carbon; red, oxygen; blue, nitrogen. Isosurface cut-off value: 0.02. (For interpretation of the references to color in this figure legend, the reader is referred to the web version of this article.)

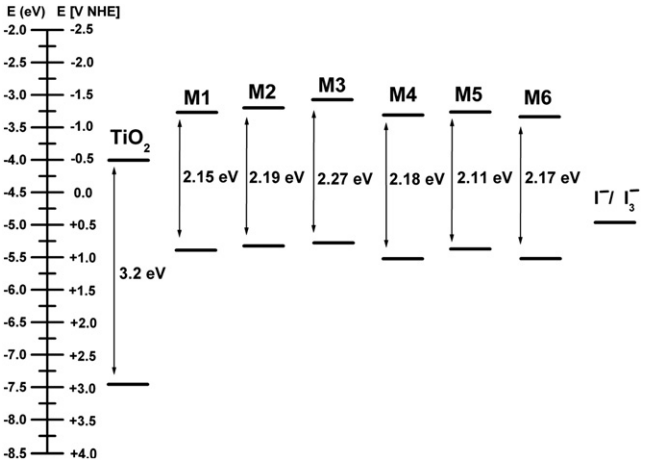

Fig. 4. Schematic representation of the band structures in DSSC dyes incorporating **M1**–**M6**. The units of the energy scale are electron volts, using the normal hydrogen electrode (NHE).

Mulliken charge separation from the carbazole units to the 2-cyanoacrylic acid moieties. The effect of the increased number of thiophene units was consistent with the computational data. Among **M1**–**M3**, the intensities of the (b) band followed the order **M2** > **M3** > **M1**. We observed a similar trend among **M4**–**M6**, with **M5** having the highest oscillator strength ($f = 2.56$).

3.3. Electrochemical properties

To evaluate the electrochemical behavior of the dyes, we investigated the cyclic voltammetry (CV) measurements; their data and plots are shown in Table 1 and Fig. S3 (see Supporting information), respectively. The $E_{ox/onset}$ values were used to calculate the HOMO levels, and the optical band gaps (E_g^{opt}, derived from the absorption onsets) were used to calculate the LUMO levels (estimated by their differences). All dyes exhibited quasi-reversible oxidation potentials attributed to the oxidation of the carbazole moieties. The measured HOMO levels were in the range of −5.35 eV to −5.75 eV (Table 1) with respect to that of iodide (−4.60 eV vs. vacuum) and thus provide negative Gibb's energy changes for the dye generation [28]. Due to their similar donor structures, the quasi-reversible oxidation potentials in all dyes were similar. The LUMO levels of all dyes were in the range of −3.09 eV to −3.6 eV, which were higher than the conduction band edge (−4.0 eV vs. vacuum). This provided an efficient thermodynamic driving force for electron injection from the excited dyes to TiO_2 conduction bands prior to radiative or nonradiative decay.

3.4. Photovoltaic performance of DSSCs based on *M1*–*M6* dyes

The photovoltaic properties of DSSCs fabricated using organic dyes as sensitizers for nanocrystalline anatase TiO_2 and an electrolyte comprising of I_2 (0.05 M)/LiI (0.5 M)/4-tert-Butylpyridine (0.5 M) in an acetonitrile solution were measured under simulated AM 1.5 irradiation (100 mW/cm^2). Fig. 5a and b present the *J*–*V* and IPCE curves of the dyes, respectively, and their corresponding data are listed in Table 3. The PCEs (η) of the dyes ranged from 2.82 to 4.82%, following the order **M1** > **M3** > **M5** > **M4** > **M2** > **M6**. Among these DSSC devices, the highest PCE was achieved for that incorporating **M1**, reaching approximately 67% of the value of η of the standard ruthenium-based N719 dye (fabricated and measured under similar conditions). The DSSC devices based on dyes **M1**, **M4**, and **M5** exhibited maximum IPCEs of approximately 65–70%,

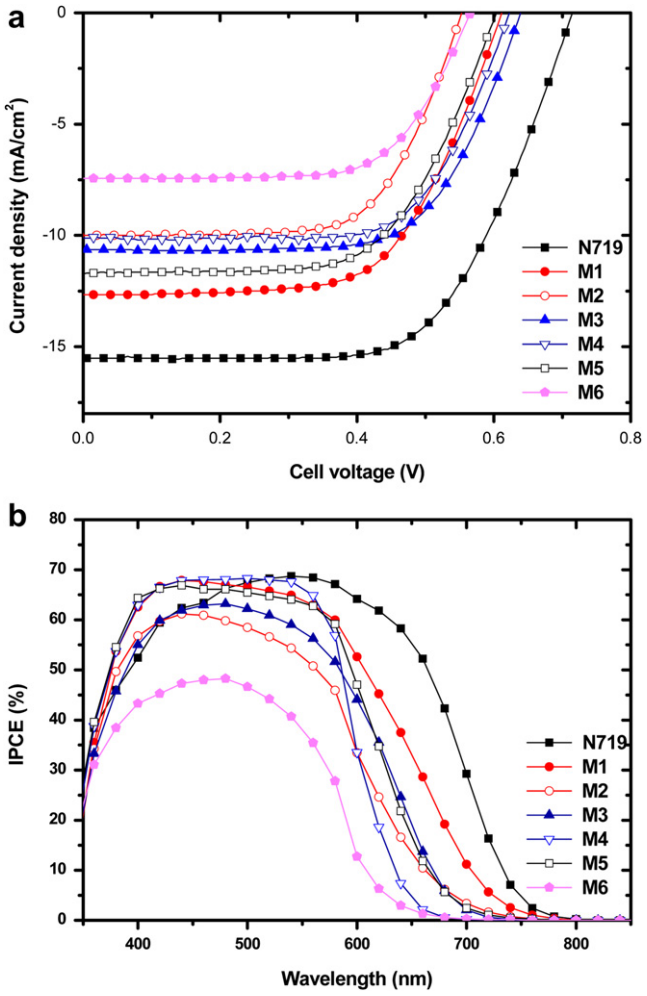

Fig. 5. (a) *J*–*V* curves and (b) IPCE plots of the dye-based DSSCs under illumination with simulated solar light (AM 1.5, 100 mW cm^{-2}). The electrolyte comprised 0.5 M LiI, 0.05 M I_2, and 0.5 M TBP.

nearly equivalent to that of the metal-based N719 dye. Nevertheless, because of the low dye loading of **M2**, the low absorption of **M3**, and the high degree of aggregation of **M6**, efficient light harvesting and injection of electrons from the excited state of these dyes to the conduction bands of TiO_2 were disfavored, causing the IPCEs of their devices to be less than 65%. The broader IPCE spectrum of **M1**, extended to the longer wavelength region, relative to that of **M3**, resulted in a higher PCE (η = 4.82%). Nevertheless, among dyes **M1**–**M6**, **M3** adsorbed to the greatest extent on the TiO_2 surface, increasing its light harvesting efficiency and, therefore, its photocurrent, even though it had the lowest absorption

Table 3
Photovoltaic parameters measured at an irradiance of 100 mW cm^{-2} AM 1.5G sunlight.

Dyes	V_{oc} [V]	J_{sc} [mA cm^{-2}]	FF	η [%]	τ_R [ms][a]
M1	0.61	12.66	0.62	4.82	0.93
M2	0.55	9.99	0.66	3.64	0.58
M3	0.64	10.63	0.67	4.55	0.66
M4	0.62	10.12	0.68	4.26	0.73
M5	0.60	11.74	0.63	4.41	0.82
M6	0.57	7.44	0.67	2.82	0.62
N719	0.72	15.65	0.64	7.19	1.28

[a] τ_R: recombination lifetime from the photovoltage measurement.

maximum [37]. As a result, **M3** overcame its shorter-wavelength absorption, due to the negative effect of its alkyl chain interactions (compared with **M1**), causing its overall PCE to be much closer to that of **M1**. In the case of **M2**, the same 3,6-functionalized carbazole donor core as that of **M1** combined with a longer conjugation length (one more thiophene unit) led to greater aggregation on the TiO_2 surface, inducing lower dye loading and restricting efficient electron injection from the excited dye to the TiO_2 conduction bands. Among the dyes **M4**–**M6** containing a planar 2,7-functionalized carbazole core, **M5** achieved the highest PCE of 4.42% (Table 3). Although we expected greater efficiency, the coplanarity and longer conjugation of the 2,7-carbazole unit of **M5** hindered its net dye adsorption (the lowest among **M1**–**M6**) and, thus, decreased its generated photocurrent. Nevertheless, the wider spectral response and higher oscillation strength of **M5** improved the net light harvesting and electron-injection efficiency upon photoexcitation of the dye and further enhanced its value of J_{sc} [44]. Aggregation on the TiO_2 surface considerably enhanced the degree of charge recombination between the injected electrons and the oxidized dye [45]. Most of the incident light was lost without photocurrent generation, resulting in a dramatically decreased PCE [the lowest value of η (2.82%) among **M1**–**M6**].

To investigate the extent of charge recombination between the oxidized dye and the redox couple, we measured the transient photovoltage at open-circuit in the presence of LiI (0.5 M) in MeCN to determine the lifetimes of the electrons photoinjected from the dyes. We estimated the average electron lifetime by fitting the decay of the open-circuit voltage transient with $\exp(-t/\tau_R)$, where t is the elapsed time and τ_R is the recombination lifetime (average time constant prior to recombination). As illustrated in Fig. 6, **M2** and **M6** provided shorter electron lifetimes (Table 3) and, thus, higher rates of charge recombination, decreasing the monochromatic quantum efficiencies and the values of J_{sc} [46]. The electron lifetimes of the other dyes were consistent with their photocurrents and PCEs. In general, the dyes **M2** and **M6** provided the lowest PCEs (3.64 and 2.82%, respectively); these dyes contained different central cores, but shared the common feature of three symmetrical thiophene units with hexyl side chains.

To determine whether the use of metal-free dyes **M1** and **M5** with high molar extinction coefficients was advantageous relative to metal-containing dye N719, we monitored the performance of nanocrystalline TiO_2-based thin film DSSCs incorporating single-layer 3- and 6-μm films of TiO_2. We also compared these results with those obtained using a double-layer 14-μm film—that is, with a 9-μm layer of 20-nm-sized particles and a 5-μm layer of 300-nm-sized light scattering particles. Figs. 7 and 8 display the IPCE curves and J–V curves, respectively, of these systems; Table 4 lists their device data. The IPCE curves of the device incorporating the N719 dye varied with respect to those of the metal-free dyes **M1** and **M5** to different extents, which were dependent on the thicknesses of the TiO_2 films. When we decreased the thickness of the TiO_2 film from 14 μm to 6 and 3 μm, the maximum IPCEs of the N719-based device decreased from approximately 65–70% to approximately 55 and 50%, respectively. In contrast, the maximum IPCEs of the **M1**- and **M5**-based devices varied negligibly upon decreasing their thicknesses (from ca. 65–70% to ca. 65 and 60%). These observations suggest that the IPCEs, molar extinction coefficients, and thicknesses of the TiO_2 films are interdependent. Table 4 reveals no significant differences in the values of J_{sc} of the DSSCs containing **M1**, **M5**, and N719 with TiO_2 films of various thicknesses. For lower IPCEs, the degree of injection of electrons from the excited states of the dyes to the conduction bands of TiO_2 decreased accordingly, thereby lowering the values of J_{sc}. In the DSSC device containing the dye N719, the value of J_{sc} decreased noticeably to 8.19 mA cm^{-2} for a single-layer TiO_2 thickness of 3 μm from 15.65 mA cm^{-2} for a double-layer thickness of 14 μm. The overall PCE of the dye N719 was compensated, however, by the higher open-circuit voltage due

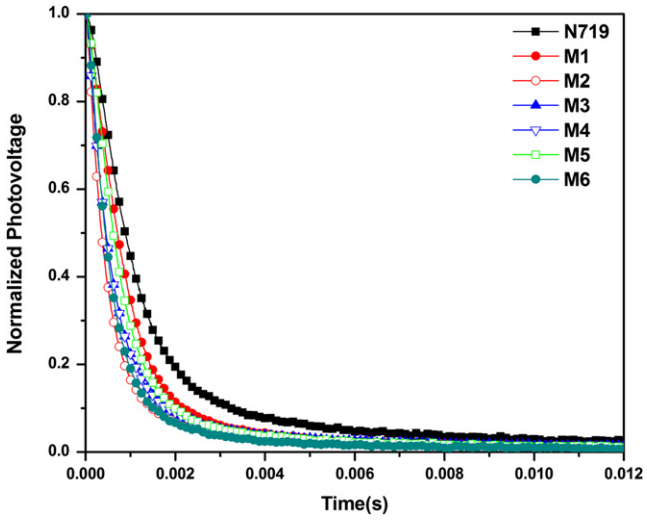

Fig. 6. Normalized electron lifetimes of the dyes **M1**–**M6** and N719 plotted with respect to the extracted charge under open-circuit conditions in the presence of LiI (0.5 M) as the electrolyte in MeCN solutions.

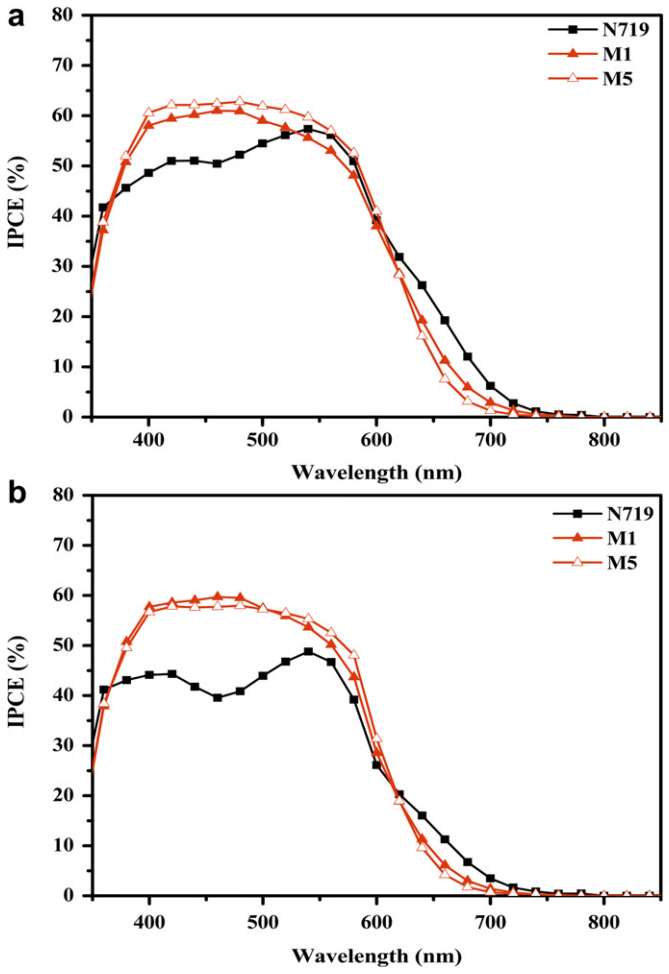

Fig. 7. IPCE spectra of **M1**, **M5**, and N719 in TiO_2 films with the thicknesses of (a) 6 μm and (b) 3 μm.

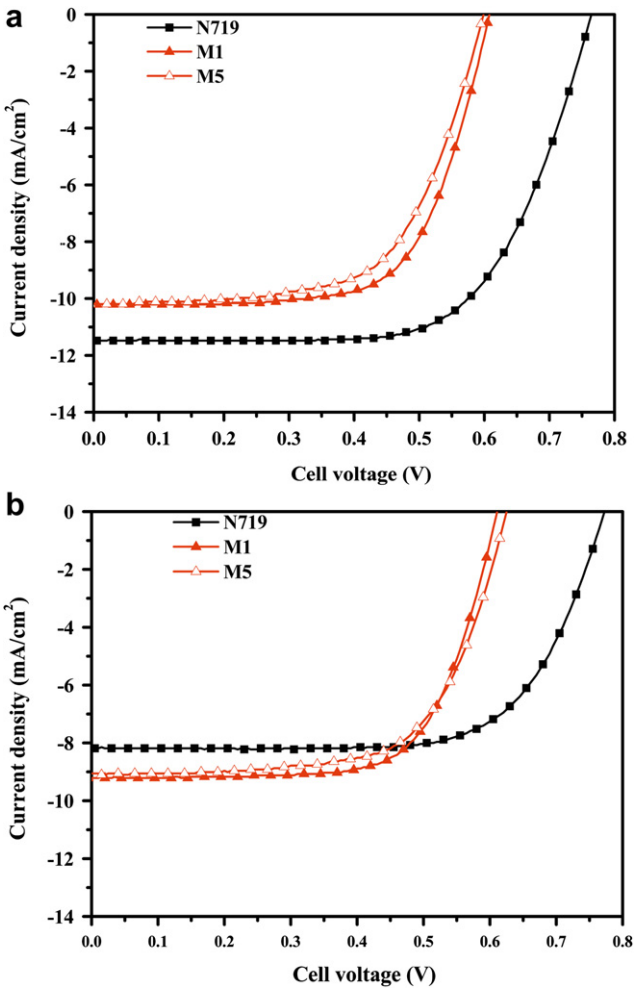

Fig. 8. *J–V* curves of DSSCs devices based on the **M1**, **M5**, and N719 dyes in TiO_2 films with the thickness of (a) 6 μm and (b) 3 μm.

to the decrease in the dark current. On the other hand, the lower dark currents in the thin films of the dyes **M1** and **M5** resulted in higher fill factors (FFs; Table 4) than those in thick films; thus, even though the values of J_{sc} decreased in thinner films, the efficiencies remained stable because of their high molar extinction coefficients.

In the double-layer 14-μm-thick devices incorporating **M1**, **M5**, and N719, the increased membrane thickness enhanced the values of J_{sc}, providing maximum PCEs of 4.82, 4.41, and 7.19%, respectively. Therefore, the FF increased upon decreasing the membrane thickness. With the higher molar extinction coefficients of the organic dyes, the PCEs (from solar to electrical energy) in the DSSCs incorporating the dyes **M1** and **M5** (in 3 μm thin films) reached 88 and 85%, respectively, of that of the device featuring the metal-based dye N719. In general, because both the CT and ICT transitions of donor–acceptor organic dyes were against the metal-to-ligand charge transfer transitions of their metal counterparts, these dyes possessed higher molar extinction coefficients that led to more-efficient light harvesting.

Table 4
Photovoltaic properties of DSSCs incorporating **M1**, **M5**, and N719 in transparent TiO_2 films of different thicknesses (single or double layers), measured under AM 1.5G irradiation (100 mW cm^{-2}).

Thickness	Dye	V_{oc} [V]	J_{sc} [mA cm^{-2}]	FF	η [%]
3 μm	**M1**	0.61	9.22	0.69	3.87
	M5	0.63	9.05	0.66	3.72
	N719	0.77	8.19	0.69	4.37
6 μm	**M1**	0.61	10.21	0.67	4.15
	M5	0.60	10.41	0.64	3.92
	N719	0.76	11.48	0.66	5.79
14 μm[a]	**M1**	0.61	12.66	0.62	4.82
	M5	0.60	11.74	0.63	4.41
	N719	0.72	15.65	0.64	7.19

[a] A double-layer of 14 μm with a layer (9 μm) of 20-nm-sized particles and a layer (5 μm) of 300 nm-sized light scattering particles.

4. Conclusions

We have synthesized two series of organic sensitizers **M1**–**M3** and **M4**–**M6** with functionalized 3,6- and 2,7-carbazole (donor) cores, respectively, connected to two anchoring cyanoacrylic acid (acceptor) termini via symmetrical conducting thiophene linkers (with or without hexyl side chains). To the best of our knowledge, the planar 2,7-carbazole cores of the dyes **M4**–**M6** have not been employed previously in the molecular design of DSSC dyes. A DSSC device based on the dye **M1** produced the highest power conversion efficiency (η) of 4.82% with an open-circuit voltage (V_{oc}) of 0.61 V, a short-circuit photocurrent density (J_{sc}) of 12.66 mA cm^{-2}, and a fill factor (FF) of 0.62 under standard AM 1.5 sunlight, with a maximum IPCE of 68%. The short electron lifetimes of the dyes **M2** and **M6** accelerated the recombination rate, however, thereby decreasing the value of η. Although suppression of π–π stacking occurred for the dyes **M1**–**M3** containing the nonplanar 3,6-carbazole core, their overall photovoltaic properties were better than those of the dyes **M4**–**M6** containing the planar 2,7-carbazole core, because of the relatively higher dye loadings and superior binding of dyes **M1**–**M3** to TiO_2 surfaces. We conclude that our novel structural design of symmetrical acceptor–donor–acceptor organic sensitizers, with variations in the number of thiophene linkers, the presence or absence of hexyl side chains on the thiophene units, and different substitution patterns (2,7 and 3,6) on the carbazole cores, can influence the net light harvesting ability, the spectral response, and, therefore, the photovoltaic properties.

Acknowledgments

We are grateful to the National Center for High-performance Computing for computer time and facilities. The financial support of this project from the National Science Council of Taiwan (ROC) through NSC 97-2113-M-009-006-MY2, National Chiao Tung University through 97W807, and Energy and Environmental Laboratories (charged by Dr. Chang-Chung Yang) in Industrial Technology Research Institute (ITRI) is acknowledged.

Appendix. Supporting information

Supporting information related to this article can be found online at doi:10.1016/j.dyepig.2011.09.012.

References

[1] Grätzel M. Photovoltaic and photoelectrochemical conversion of solar energy. Phil Trans R Soc A 2007;365:993.
[2] (a) Katzenstein W, Apt J. Air emissions due to wind and solar power. Environ Sci Technol 2009;43:253;
(b) Schafer AI, Broeckmann A, Richards BS. Development and characterization of a photovoltaic hybrid membrane system. Environ Sci Technol 2007;41:998.
[3] Tang CW. 2-Layer organic photovoltaic cell. Appl Phys Lett 1986;48:183.
[4] Liu R. Imaging of photoinduced interfacial charge separation in conjugated polymer/semiconductor nanocomposites. J Phys Chem C 2009;11:9368.
[5] Prezhdo OV, Duncan WR, Prezhdo V. Dynamics of the photoexcited electron at the chromophore-semiconductor interface. Acc Chem Res 2008;41:339.

[6] Peumans P, Bulovic V, Forrest SR. Efficient photon harvesting at high optical intensities in ultrathin organic double heterostructure photovoltaic diodes. Appl Phys Lett 2000;76:2650.
[7] Yu G, Gao J, Hummelen JC, Wudl F, Heeger AJ. Polymer photovoltaic cells: enhanced efficiencies via a network of internal donor–acceptor heterojunctions. Science 1995;270:1789.
[8] Halls JJM, Walsh CA, Greenham NC, Marseglia EA, Friend RH, Moratti SC, et al. Efficient photodiodes from interpenetrating polymer networks. Nature 1995; 376:498.
[9] (a) Li J, Grimsdale AC. Carbazole-based polymers for organic photovoltaic devices. Chem Soc Rev 2010;39:2399;
(b) Wang HL, Wang XY, Wang L, Wang HL, Liu AH. Theoretical study on the optical properties for 2,7- and 3,6-linked carbazole trimers by time-dependent density functional theory. Chin J Struct Chem 2007;26:413.
[10] (a) Li KC, Huang JH, Hsu YC, Huang PJ, Chu CW, Lin JT, et al. Tunable novel cyclopentadithiophene-based copolymers containing various numbers of bithiazole and thienyl units for organic photovoltaic cell applications. Macromolecules 2009;42:3681;
(b) Jenekhe SA, Yi S. Efficient photovoltaic cells from semiconducting polymer heterojunctions. Appl Phys Lett 2000;77:2635;
(c) Padhy H, Sahu D, Chiang IH, Patra D, Kekuda D, Chu CW, et al. J Mater Chem 2011;21:1196.
[11] Granström M, Petritsch K, Arias AC, Lux A, Andersson MR, Friend RH. Laminated fabrication of polymeric photovoltaic diodes. Nature 1998; 395:257.
[12] Huynh WU, Dittmer JJ, Alivisatos AP. Hybrid nanorod-polymer solar cells. Science 2002;295:2425.
[13] (a) Freeman AW, Urvoy M, Criswell ME. Triphenylphosphine-mediated reductive cyclization of 2-nitrobiphenyls: a practical and convenient synthesis of carbazoles. J Org Chem 2005;70:5014;
(b) Blouin N, Michaud A, Leclerc M. A low-bandgap poly(2,7-carbazole) derivative for use in high-performance solar cells. Adv Mater 2007;19:2295;
(c) Tomkeviciene A, Grazulevicius JV, Jankauskas V. High hole mobilities in the amorphous films of 2,7-di(9-carbazolyl)-9-(2-ethylhexyl)carbazole. Chem Lett 2008;37:344;
(d) Blouin N, Michaud A, Gendron D, Wakim S, Blair E, Neagu-Plesu R, et al. Toward a rational design of poly(2,7-carbazole) derivatives for solar cells. J Am Chem Soc 2008;130:732.
[14] (a) O'Regan B, Grätzel M. A low-cost, high-efficiency solar cell based on dye-sensitized colloidal TiO_2 films. Nature 1991;353:737;
(b) Grätzel M. Photoelectrochemical cells. Nature 2001;414:338.
[15] (a) Nazeeruddin MK, Pechy P, Renouard T, Zakeeruddin SM, Humphry-Baker R, Comte P, et al. Engineering of efficient panchromatic sensitizers for nanocrystalline TiO_2-based solar cells. J Am Chem Soc 2001;123:1613;
(b) Nazeeruddin MK, Zakeeruddin SM, Humphry-Baker R, Jirousek M, Liska P, Vlachopoulos N, et al. Acid-Base equilibria of (2,2′-bipyridy-4,4′-dicarboxylic acid) ruthenium(II) complexes and the effect of protonation on charge-transfer sensitization of nanocrystalline titania. Inorg Chem 1999;38:6298.
[16] (a) Nazeeruddin MK, DeAngelis F, Fantacci S, Selloni A, Viscardi G, Liska P, et al. Combined experimental and DFT-TDDFT computational study of photoelectrochemical cell ruthenium sensitizers. J Am Chem Soc 2005;127:16835;
(b) Nusbaumer H, Zakeeruddin SM, Moser JE, Grätzel M. An alternative efficient redox couple for the dye-sensitized solar cell system. Chem Eur J 2003;9:3756.
[17] (a) Chen CY, Chen JG, Wu SJ, Li JY, Wu CG, Ho KC. Multi-functionalized ruthenium based super-sensitizers for high efficient dye-sensitized solar cells. Angew Chem Int Ed 2008;47:7342;
(b) Yin JF, Bhattacharya D, Hsu YC, Tsai CC, Lu KL, Lin HC, et al. Enhanced photovoltaic performance by synergism of light-cultivation and electronic localization for highly efficient dye-sensitized solar cells. J Mater Chem 2009; 19:7036.
[18] Yin JF, Chen JG, Lu ZZ, Ho KC, Lin HC, Lu KL. Towards optimization of oligothiophene antennas: new ruthenium sensitizers with excellent performance for dye-sensitized solar cells. Chem Mater 2010;22:4392.
[19] Gao F, Wang Y, Zhang J, Shi D, Wang M, Humphry-Baker R, et al. A new heteroleptic ruthenium sensitizer enhances the absorptivity of mesoporous titania film for a high efficiency dye-sensitized solar cell. Chem Commun; 2008:2635.
[20] (a) Ning Z, Zhang Q, Wu W, Pei H, Liu B, Tian H. Starburst triarylamine based dyes for efficient dye-sensitized solar cells. J Org Chem 2008;73:3791;
(b) Zhou G, Pschirer N, Schöneboom JC, Eickemeyer F, Baumgarten M, Müllen K. Ladder-type pentaphenylene dyes for dye-sensitized solar cells. Chem Mater 2008;20:1808;
(c) Wiberg J, Marinado T, Hagberg DP, Sun L, Hagfeldt A, Albinsson B. Distance and driving force dependencies of electron injection and recombination dynamics in organic dye-sensitized solar cells. J Phys Chem B 2010;114: 14358;
(d) Wu W, Yang J, Hua J, Tang J, Zhang L, Long Y, et al. Efficient and stable dye-sensitized solar cells based on phenothiazine sensitizers with thiophene units. J Mater Chem 2010;20:1772;
(e) Choi H, Raabe I, Kim D, Teocoli F, Kim C, Song K, et al. High molar extinction coefficient organic sensitizers for efficient dye-sensitized solar cells. Chem Eur J 2010;16:1193.
[21] (a) Koumura N, Wang ZS, Mori S, Miyashita M, Suzuki E, Hara K. Alkyl-functionalized organic dyes for efficient molecular photovoltaics. J Am Chem Soc 2006;128:14256;
(b) Bessho T, Yoneda E, Yum JH, Guglielmi M, Tavernelli I, Imai H, et al. New paradigm in molecular engineering of sensitizers for solar cell applications. J Am Chem Soc 2009;131:5930;
(c) Thomas KRJ, Singh P, Baheti A, Hsu YC, Ho KC, Lin JT. Electro-optical properties of new anthracene based organic dyes for dye-sensitized solar cells. Dyes Pigm 2011;91:33.
[22] (a) Shi D, Cao Y, Pootrakulchote N, Yi Z, Xu M, Zakeeruddin SM, et al. New organic sensitizer for stable dye-sensitized solar cells with solvent-free ionic liquid electrolytes. J Phys Chem C 2008;112:17478;
(b) Teng C, Yang X, Yang C, Li S, Cheng M, Hagfeldt A, et al. Influence of triple bonds as π-spacer units in metal-free organic dyes for dye-sensitized solar cells. J Phys Chem C 2010;114:9101;
(c) Choi H, Kim JJ, Song K, Ko J, Nazeeruddin MK, Gratzel M. Molecular engineering of panchromatic unsymmetrical squaraines for dye-sensitized solar cell applications. J Mater Chem 2010;20:3280;
(d) Hsieh CP, Lu HP, Cheu CL, Lee CW, Chuang SH, Mai CL, et al. Synthesis and characterization of porphyrin sensitizers with various electron-donating substituents for highly efficient dye-sensitized solar cells. J Mater Chem 2010;20:1127;
(e) Maeda T, Nakao H, Kito H, Ichinose H, Yagi S, Nakazumi H. Far-red absorbing squarylium dyes with terminally connected electron-accepting units for organic dye-sensitized solar cells. Dyes Pigm 2011;90:275.
[23] (a) Chen KF, Hsu YC, Wu Q, Yeh MCP, Sun SS. Structurally simple dipolar organic dyes featuring 1,3-cyclohexadiene conjugated unit for dye-sensitized solar cells. Org Lett 2009;11:377;
(b) Xu W, Peng B, Chen J, Liang M, Cai F. New triphenylamine-based dyes for dye-sensitized solar cells. J Phys Chem C 2008;112:874;
(c) Jiang X, Marinado T, Gabrielsson E, Hagberg DP, Sun L, Hagfeldt A. Structural modification of organic dyes for efficient co-adsorbent-free dye-sensitized solar cells. J Phys Chem C 2010;114:2799;
(d) Mishra A, Fischer MKR, Bäuerle P. Metal-free organic dyes for dye-sensitized solar cells: from structure: property relationships to design rules. Angew Chem Int Ed 2009;48:2474;
(e) Tian H, Yang X, Cong J, Chen R, Teng C, Liu J, et al. Effect of different electron donating groups on the performance of dye-sensitized solar cells. Dyes Pigm 2010;84:62.
[24] (a) Park SS, Won YS, Choi YC, Kim JH. Molecular design of organic dyes with double electron acceptor for dye-sensitized solar cell. Energy Fuels 2009;23: 3732;
(b) Chen Y, Zeng Z, Li C, Wang W, Wang X, Zhang B. Highly efficient co-sensitization of nanocrystalline TiO_2 electrodes with plural organic dyes. New J Chem 2005;29:773;
(c) Abbotto A, Manfredi N, Marinzi C, DeAngelis F, Mosconi E, Yum JH, et al. Dibranched di-anchoring organic dyes for dye-sensitized solar cells. Energy Environ Sci 2009;2:1094;
(d) Tan S, Zhai J, Fang H, Jiu T, Ge J, Li Y, et al. Novel carboxylated oligothiophenes as sensitizers in photoelectric conversion systems. Chem Eur J 2005; 11:6272;
(e) Sahu D, Padhy H, Patra D, Yin JF, Hsu YC, Lin JT, et al. Synthesis and applications of novel acceptor–donor–acceptor organic dyes with dithienopyrrole- and fluorene-cores for dye-sensitized solar cells. Tetrahedron 2011; 67:303.
[25] Heredia D, Natera J, Gervaldo M, Otero L, Fungo F, Lin CY, et al. Intramolecular hydrogen bonds preorganize an aryl-triazole receptor into a crescent for chloride binding. Org Lett 2010;12:12.
[26] Wang ZS, Koumura N, Cui Y, Takahashi M, Sekiguchi H, Mori A, et al. Hexylthiophene-functionalized carbazole dyes for efficient molecular photovoltaics: tuning of solar-cell performance by structural modification. Chem Mater 2008;20:3993.
[27] Koumura N, Wang ZS, Miyashita M, Uemura Y, Sekiguchi H, Cui Y, et al. Substituted carbazole dyes for efficient molecular photovoltaics: long electron lifetime and high open circuit voltage performance. J Mater Chem 2009;19:4829.
[28] (a) Liu Y, Xiang N, Feng X, Shen P, Zhou W, Weng C, et al. Thiophene-linked porphyrin derivatives for dye-sensitized solar cells. Chem Commun; 2009:2499;
(b) Tian H, Yang X, Cong J, Chen R, Liu J, Hao Y, et al. Tuning of phenoxazine chromophores for efficient organic dye-sensitized solar cells. Chem Commun; 2009:6288.
[29] (a) Chen CY, Wu SJ, Wu CG, Chen JG, Ho KC. A ruthenium complex with superhigh light harvesting capacity for dye-sensitized solar cells. Angew Chem Int Ed 2006;45:5822;
(b) Huang CY, Hsu YC, Chen JG, Suryanarayanan V, Lee KM, Ho KC. The effects of hydrothermal temperature and thickness of TiO_2 film on the performance of a dye-sensitized solar cell. Sol Energy Mater Sol Cell 2006;90:2391;
(c) Lee KM, Suryanarayanan V, Ho KC. The influence of surface morphology of TiO_2 coating on the performance of dye-sensitized solar cells. Sol Energy Mater Sol Cell 2006;90:2398.
[30] (a) Becke AD. Density-functional thermochemistry. III. The role of exact exchange. J Chem Phys 1993;98:5648;
(b) Lee C, Yang W, Par RG. Development of the Colle–Salvetti correlation-energy formula into a functional of the electron density. Phys Rev B 1988; 37:785.
[31] (a) Hey PJ, Wadt WR. Ab initio effective core potentials for molecular calculations. Potentials for the transition metal atoms Sc to Hg. J Chem Phys 1985; 82:270;

(b) Wadt WR, Hey PJ. Ab initio effective core potentials for molecular calculations. Potentials for main group elements Na to Bi. J Chem Phys 1985;82:284.
[32] Pople JA. Gaussian 03, revision E01. Wallingford CT: Gaussian Inc; 2004.
[33] O'Boyle NM, Vos J. GaussSum1.0. Dublin Ireland: Dublin City University. Available at: http://gausssumsourceforgenet; 2005.
[34] (a) Kim D, Lee JK, Kang SO, Ko J. Molecular engineering of organic dyes containing N-aryl carbazole moiety for solar cell. Tetrahedron 2007;63:1913;
(b) Yue W, Zhao Y, Shao S, Tian H, Xie Z, Geng Y, et al. Novel NIR-absorbing conjugated polymers for efficient polymer solar cells: effect of alkyl chain length on device performance. J Mater Chem 2009;19:2199.
[35] Remmers M, Muller B, Martin K, Rader HJ. Poly(p-phenylene)s. Synthesis, optical properties and quantitative analysis with HPLC and MALDI-TOF mass spectrometry. Macromolecules 1999;32:1073.
[36] (a) Yen YS, Hsu YC, Lin JT, Chang CW, Hsu CP, Yin DJ. Pyrrole-based organic dyes for dye-sensitized solar cells. J Phys Chem C 2008;112:12557;
(b) Ko S, Choi H, Kang MS, Hwang H, Ji H, Kim J, et al. Silole-spaced triarylamine derivatives as highly efficient organic sensitizers in dye-sensitized solar cells (DSSCs). J Mater Chem 2010;20:2391.
[37] (a) Liang M, Xu W, Cai F, Chen P, Peng B, Chen J, et al. New triphenylamine-based organic dyes for efficient dye-sensitized solar cells. J Phys Chem C 2007;111:4465;
(b) Thomas KRJ, Hsu YC, Lin JT, Lee KM, Ho KC, Lai CH, et al. 2,3-Disubstituted thiophene-based organic dyes for solar cells. Chem Mater 2008;20:1830;
(c) Wang ZS, Hara K, Danoh Y, Kasada C, Shinpo A, Suga S, et al. Photophysical and (photo)electrochemical properties of a coumarin dye. J Phys Chem B 2005;109:3907.
[38] Lohwasser RH, Bandara J, Thelakkat M. Tailor-made synthesis of poly(3-hexylthiophene) with carboxylic end groups and its application as a polymer sensitizer in solid-state dye-sensitized solar cells. J Mater Chem 2009;19:4126.
[39] Mann JR, Gannon MK, Fitzgibbons TC, Detty MR, Watson DF. Optimizing the photocurrent efficiency of dye-sensitized solar cells through the controlled aggregation of chalcogenoxanthylium dyes on nanocrystalline titania films. J Phys Chem C 2008;112:13057.
[40] Chen CH, Hsu YC, Chou HH, Thomas KRJ, Lin JT, Hsu CP. Dipolar compounds containing fluorene and a heteroaromatic ring as the conjugating bridge for high-performance dye-sensitized solar cells. Chem Eur J 2010;16:3184.
[41] Li R, Lv X, Shi D, Zhou D, Cheng Y, Zhang G, et al. Dye-sensitized solar cells based on organic sensitizers with different conjugated linkers: furan, bifuran, thiophene, bithiophene, selenophene, and biselenophene. J Phys Chem C 2009;113:7469.
[42] Burfeindt B, Hannappel T, Storck W, Willig F. Comparison of dye- and semiconductor-sensitized porous nanocrystalline liquid junction solar cells. J Phys Chem C 2008;112:17778.
[43] Tian H, Yang X, Chen R, Pan Y, Li L, Hagfeldt A, et al. Phenothiazine derivatives for efficient organic dye-sensitized solar cells. Chem Commun; 2007:3741.
[44] (a) Wang ZS, Cui Y, Danoh Y, Kasada C, Shinpo A, Hara K. Thiophene-functionalized coumarin dye for efficient dye-sensitized solar cells: electron lifetime improved by coadsorption of deoxycholic acid. J Phys Chem C 2007;111:7224;
(b) Hagberg DP, Jiang X, Gabrielsson E, Linder M, Marinado T, Brinck T, et al. Symmetric and unsymmetric donor functionalization. comparing structural and spectral benefits of chromophores for dye-sensitized solar cells. J Mater Chem 2009;19:7232.
[45] (a) Liu D, Fessenden RW, Hug GL, Kamat PV. Dye capped semiconductor nanoclusters. Role of back electron transfer in the photosensitization of SnO_2 nanocrystallites with cresyl violet aggregates. J Phys Chem B 1997;101:2583;
(b) Qu S, Wu W, Hua J, Kong C, Long Y, Tian H. New diketopyrrolopyrrole (DPP) dyes for efficient dye-sensitized solar cells. J Phys Chem C 2010;114:1343.
[46] Wong DKP, Ku CH, Chen YR, Chen GR, Wu JJ. Enhancing electron collection efficiency and effective diffusion length in dye-sensitized solar cells. Chem Phys Chem 2009;15:2698.